First-principles determination of Heisenberg Hamiltonian parameters for the spin-$\frac{1}{2}$ kagome antiferromagnet $ZnCu_3(OH)_6Cl_2$

Harald O. Jeschke,* Francesc Salvat-Pujol, and Roser Valentí

Institut für Theoretische Physik, Goethe-Universität Frankfurt, Max-von-Laue-Strasse 1, 60438 Frankfurt am Main, Germany

(Received 8 March 2013; revised manuscript received 10 July 2013; published 5 August 2013)

Herbertsmithite [$ZnCu_3(OH)_6Cl_2$] is often discussed as the best realization of the highly frustrated antiferromagnetic kagome lattice known so far. We employ density functional theory (DFT) calculations to determine eight exchange coupling constants of the underlying Heisenberg Hamiltonian. We find the nearest-neighbor coupling J_1 to exceed all other couplings by far. However, next-nearest-neighbor kagome layer couplings of $0.019J_1$ and interlayer couplings of up to $-0.035J_1$ slightly modify the perfect antiferromagnetic kagome Hamiltonian. Interestingly, the largest interlayer coupling is ferromagnetic, even without Cu impurities in the Zn layer. In addition, we validate our DFT approach by applying it to kapellasite, a polymorph of herbertsmithite, which is known experimentally to exhibit competing exchange interactions.

DOI: 10.1103/PhysRevB.88.075106 PACS number(s): 75.10.Kt, 71.20.−b, 75.10.Jm, 75.30.Et

Quantum spin liquids have fascinated physicists for decades, as this exotic ground state constitutes a novel state of matter.[1] The magnetic moments in a spin liquid do not order even at extremely low temperature due to a high degree of frustration in the magnetic system. Typical examples for lattices that lead to frustration of antiferromagnetic interactions are triangular, pyrochlore, and kagome lattices. While experimental realizations of quantum spin liquids have long been scarce, in particular, the discovery[2] of the perfect kagome lattice realization in herbertsmithite has led to considerable excitement.[3] In the eight years since the discovery of the $S = \frac{1}{2}$ kagome antiferromagnet nature of $ZnCu_3(OH)_6Cl_2$, numerous experiments have been performed to ascertain the spin liquid ground state of herbertsmithite, its properties, and excitations.[4,5] In particular, measurements of the magnetic susceptibility[6] show antiferromagnetic couplings of the order $J \approx 17$ meV ($\sim$190 K) and no magnetic ordering down to 50 mK. Muon spin rotation measurements[7] confirm the absence of magnetic ordering and inelastic neutron scattering experiments[8,9] find that fractionalized quantum excitations are present in $ZnCu_3(OH)_6Cl_2$. More recently, nonideality of the realization of the kagome Heisenberg Hamiltonian in herbertsmithite due to additional interactions and in the form of site disorder has been the focus of many studies.[5] While defects within the kagome layer are detected in nuclear magnetic resonance[10] but not in recent x-ray scattering measurements,[11] Cu impurities on interlayer Zn sites seem to play a role.[11] Low-temperature deviations between theory for the kagome antiferromagnet and experimental susceptibilities as well as anisotropies in thermodynamic quantities[12] point to a small nonzero Dzyaloshinskii-Moriya interaction.[13,14] Evidence of this interaction has been found in electron spin resonance measurements.[15,16] However, the experimental and theoretical discussion about the Hamiltonian correctly describing herbertsmithite is far from settled.

Therefore we undertake an effort to determine the parameters of the underlying Heisenberg Hamiltonian using all-electron density functional theory (DFT) methods. We will show in this paper that the exchange coupling constants from first principles corroborate that $ZnCu_3(OH)_6Cl_2$ is a near-perfect realization of a kagome antiferromagnet with a dominant coupling of $J_1 = 182$ K. However, there are small corrections to this picture. A next-nearest-neighbor coupling in the kagome layer of $0.019J_1$ and in particular, some interplanar couplings between $-0.035J_1$ and $0.029J_1$ could actually be relevant for the nature and excitations of the spin liquid ground state in herbertsmithite.

We perform density functional theory calculations with the full potential local orbital (FPLO) basis set[17] using the generalized gradient approximation (GGA)[18] and GGA + U functionals. The exchange couplings J_i are obtained from total energy calculations for different Cu spin configurations in supercells of various sizes.[19] Before proceeding to herbertsmithite, we test our methods on kapellasite, a polymorph of herbertsmithite, which has been investigated before, both theoretically[20] and experimentally.[21] We use the structure of kapellasite as given in Ref. 22 and determine the hydrogen position by relaxation.[23] The structure is shown in Fig. 1. We create two different supercells: a $2 \times 1 \times 2$ supercell with $P\bar{1}$ symmetry and 10 inequivalent Cu positions with the purpose of resolving four interlayer couplings, and a $2 \times 2 \times 1$ supercell with $P1$ symmetry that provides symmetry inequivalent third nearest neighbors in the kagome plane. Using GGA + U with $U = 6$ eV and $J = 1$ eV, we find two significant couplings, $J_1 = -14.2$ K and $J_d = 24.0$ K (see Table I). Other couplings, such as J_2, are significantly smaller (around 1 K), and we find interlayer couplings to be negligible (see Appendix A). Note that the numbers we give are converged to sub-Kelvin precision with our choice of spin configurations; however, different sets of spin configurations will lead to slightly different values so that we estimate the uncertainty of the exchange constants for both compounds discussed in this work to be around 1 K. Systematic studies on the influence of the choice of exchange and correlation functional and other technical variations in the DFT determination of exchange couplings have been performed by some of us in Refs. 19 and 24. Table I is in very good agreement with the observation of Ref. 21 that experimental data are compatible with a J_1-J_d model with $J_1 = -15.0(4)$ K and $J_d = 12.7(3)$ K. Note that the ratio between J_1 and J_d depends on the choice of U, as the antiferromagnetic J_d in particular is inversely proportional to U (see Appendix A). Even more recently,

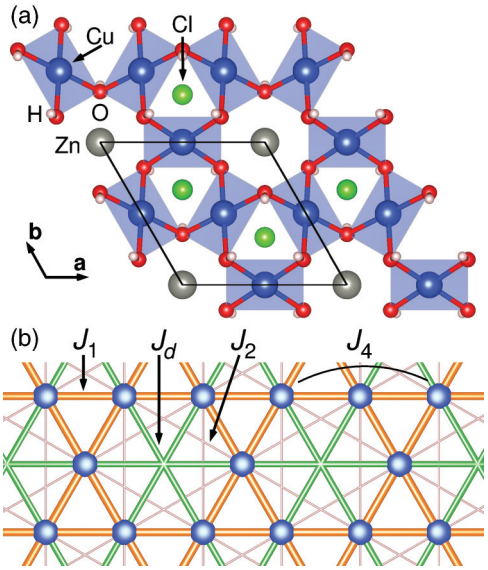

FIG. 1. (Color online) (a) Crystal structure of kapellasite, viewed along the **c** direction. (b) Kagome lattice formed by the Cu sites in (a). Note that J_d and J_4 exchange paths both correspond to a distance of 6.3 Å, but while J_4 points precisely along a nearest-neighbor bond, J_d cuts diagonally across a Cu hexagon with nonmagnetic Zn in the center.

the high-temperature series expansion method was refined to fit both magnetic susceptibility and specific heat data, yielding the set of parameters $J_1 = -12$ K, $J_2 = -4$ K, $J_d = 15.6$ K.[25] Thus we can proceed with some confidence to analyze the Heisenberg Hamiltonian parameters of herbertsmithite.

We use the structure of $ZnCu_3(OH)_6Cl_2$ (herbertsmithite) with the $R\,\bar{3}m$ space group determined by Shores *et al.*,[2] which is shown in Fig. 2(a). A big difference with respect to the polymorph kapellasite is that Zn is now between kagome layers rather than in the centers of its hexagons. In Fig. 3 we present the band structure and density of states. At the Fermi level, we find Cu $3d$ states which hybridize with O $2p$ and Cl $3p$ states. As expected, Zn plays no role at E_F. Note that the Dirac-point-like feature at K for an energy of 0.2 eV above the Fermi level becomes an avoided crossing with a tiny gap in a fully relativistic calculation. Based on our experience with azurite, another complex quantum spin system containing Cu^{2+} ions,[19] and the fact that kapellasite, the polymorph of herbertsmithite briefly analyzed above, was shown to have longer ranged competing interactions,[21] we determine all exchange constants

TABLE I. Exchange coupling constants for $ZnCu_3(OH)_6Cl_2$ (kapellasite) determined from total energies of five different spin configurations in a $2 \times 2 \times 1$ supercell (nn = nearest neighbor).

Name	d_{Cu-Cu}	Type	J_i (K) $U = 6$ eV
J_1	3.15	Kagome nn	−14.2
J_2	5.45596	Kagome 2nd nn	−0.7
J_4	6.3	Kagome 3rd nn	−0.3
J_d	6.3	Kagome 3rd nn	24.0

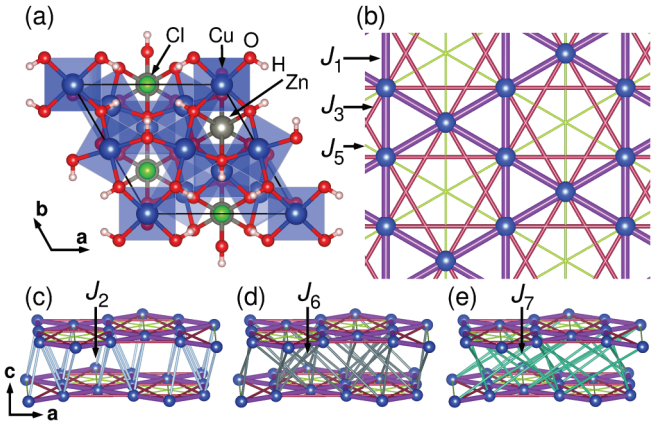

FIG. 2. (Color online) (a) Crystal structure of herbertsmithite $ZnCu_3(OH)_6Cl_2$, viewed along the c direction. (b) Kagome lattice formed by the Cu sites in (a). Exchange paths between nearest, next-nearest, and third-nearest neighbors within the kagome lattice are shown. (c)–(e) Three interkagome layer exchange pathways.

up to Cu-Cu distances of 8.6 Å. In order to allow for determination of the diagonal coupling in the kagome lattice J_5, we double the unit cell along **a** and prepare a structure with $P\,m$ space group and 12 inequivalent Cu sites. As appropriate for Cu, we employ a GGA + U exchange correlation functional with $U = 6$ eV, $J = 1$ eV and atomic-limit double-counting correction.[19] Total energies for nine different spin configurations allow us to calculate the eight exchange coupling constants listed in Table II. The three couplings within the kagome layer are shown in Fig. 2(b), and the geometry of the three most important interlayer couplings is presented in Figs. 2(c)–2(e). To avoid confusion, we number the coupling constants J_i strictly according to ascending Cu-Cu distances. While the absolute values of the exchange constants obtained from these calculations are dependent on the choice of the U

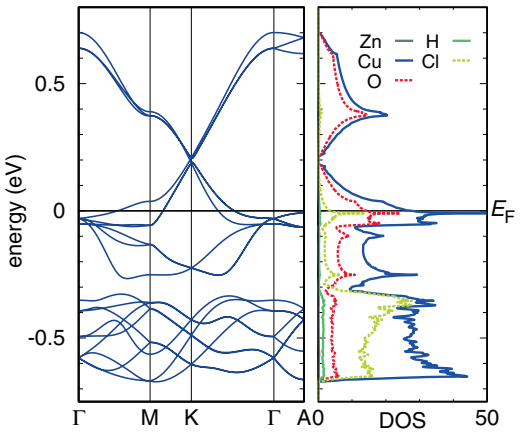

FIG. 3. (Color online) Band structure and density of states of $ZnCu_3(OH)_6Cl_2$ calculated with GGA exchange correlation functional. High-symmetry points of the $P\,\bar{3}m$ space group are $M = (\frac{1}{2},0,0)$, $K = (\frac{1}{3},\frac{1}{3},0)$, and $A = (0,0,\frac{1}{2})$ in units of the reciprocal lattice vectors. DOS is given in states per electronvolt per unit cell (containing three formula units).

TABLE II. Exchange coupling constants for $ZnCu_3(OH)_6Cl_2$ (herbertsmithite) determined from total energies of nine different spin configurations. Energies were calculated with GGA + U functional at $U = 6$ eV, $J = 1$ eV and with atomic-limit double-counting correction.

Name	d_{Cu-Cu}	Type	J_i (K) $U = 6$ eV
		Kagome layer couplings	
J_1	3.4171	Kagome nn	182.4
J_3	5.91859	Kagome 2nd nn	3.4
J_5	6.8342	Kagome 3rd nn	−0.4
		Interlayer couplings	
J_2	5.07638	Interlayer 1st nn	5.3
J_4	6.11933	Interlayer 2nd nn	−1.5
J_6	7.00876	Interlayer 3rd nn	−6.4
J_7	8.51328	Interlayer 4th nn	3.0
J_9	9.17347	Interlayer 6th nn	2.5

value in the GGA + U calculations, as already pointed out for kapellasite, one expects that the antiferromagnetic exchange constants follow a $1/U$ law while the ferromagnetic exchange constants should be less sensitive to the U value. This trend is also observed in the case of herbertsmithite when we compare the exchange constants obtained for $U = 6$ eV, $U = 7$ eV, and $U = 8$ eV (see Appendix B). In order to also have a quantitative description of the exchange constants and not only ratios, we take as reference the results obtained for $U = 6$ eV, guided by the experience with other copper-based materials as mentioned above.

Within the kagome layer, the most important correction to the presently discussed Hamiltonian for herbertsmithite is the next-nearest-neighbor coupling J_3. Theoretical investigations of the kagome lattice with nearest- and next-nearest neighbor interactions indicate that the nature of the spin liquid ground state could depend on such a next-nearest coupling.[26,27] Messio *et al.*[28] have even extended the range of the couplings to the third-nearest neighbor across a hexagon; our set of parameters would put herbertsmithite in the $q = 0$ spin liquid phase, in agreement with Ref. 9. Very recently, the Heisenberg model on the kagome lattice with nearest and next-nearest neighbor couplings has been studied with a pseudofermion functional renormalization group method;[29] very good agreement with the inelastic neutron scattering experiment of Ref. 9 is reached for the next-nearest-neighbor interaction in the plane $J_3 = 0.017J_1$, which is very close to our value.

Now we come to the interlayer couplings. First of all, it is important to note that while each Cu site has four interactions via J_1, four via J_3, and six via J_5, the interlayer bonds are numerous: There are four J_2 bonds, six J_4 bonds, eight J_6 bonds, six J_7 bonds, and six J_9 bonds. Interestingly, we find J_2 to be an antiferromagnetic interlayer coupling of size $0.029J_1$, and J_6 a ferromagnetic interlayer coupling of size $-0.035J_1$. Previous studies based on the spin-rotation-invariant Green's function method showed that a stacked kagome system remains short-range ordered, independent of the sign and strength of the interlayer coupling.[30] We have performed a first test of the relevance of the interlayer couplings for susceptibility and specific heat using high-temperature series expansion.[31] This method has been very useful to discuss the kagome lattice Heisenberg model,[32] as well as various additional terms.[33] We find that at least in the region of applicability of this method, the effect of interlayer couplings is noticeable. We hope that our results inspire more precise many-body calculations that could establish the consequences of interlayer couplings for the low-temperature properties of herbertsmithite

In summary, our *ab initio*-based analysis of the Cu-Cu exchange coupling constants in kapellasite and herbertsmithite provides a detailed description of these materials. Our results for the dominant interactions are in excellent agreement with experiments. Moreover, we are able to resolve the strength and sign of weaker, but not negligible, exchange interactions that were not known until now and are important for understanding the behavior of these materials at low temperatures. Both polymorphs, even though they are realizations of a perfect kagome lattice, show a few remarkable differences. The nearest-neighbor Cu-Cu exchange interaction is strongly antiferromagnetic in herbertsmithite (∼190 K) and weakly ferromagnetic in kapellasite (∼−13 K) because the Cu-O-Cu angle in herbertsmithite is 119° compared to 106° in kapellasite. Kapellasite shows a significant antiferromagnetic fourth-nearest-neighbor coupling along the diagonal of the Cu hexagon (J_d), which is negligible in herbertsmithite since the exchange path in kapellasite is through the in-plane Zn situated in the center of the hexagons. Also, the stacking of the kagome layers in both polymorphs is crucial for understanding the interlayer exchange couplings. In kapellasite, the kagome layers are stacked in a similar fashion as in the layered TiOCl (Ref. 34) or Cs_2CuCl_4,[24] where interactions are mostly of van der Waals nature. In this situation, the interlayer couplings are comparatively small (see Appendix B). In contrast, in herbertsmithite the interlayer Cu-Cu couplings are partly through Zn orbitals. This leads to relatively significant antiferromagnetic (J_2) and ferromagnetic (J_6) interlayer couplings. Nevertheless, the ratio between the dominant intralayer coupling J_1 and the dominant interlayer coupling remains large enough for this system to be considered a very good realization of a two-dimensional kagome lattice and only at low temperatures should the smaller J_i become important. This and the importance of couplings other than the dominant ones for the spin liquid behavior in these materials should be investigated in the future. In particular, it would be interesting to determine also the couplings of the Dzyaloshinskii-Moriya and ring exchange terms in the Hamiltonian from first principles.

TABLE III. Exchange coupling constants for kapellasite determined from total energies of five different spin configurations in a $2 \times 2 \times 1$ supercell.

Name	d_{Cu-Cu}	Type	J_i (K) $U = 6$ eV	J_i (K) $U = 7$ eV	J_i (K) $U = 8$ eV
J_1	3.15	Kagome nn	−14.2	−13.4	−12.6
J_2	5.45596	Kagome 2nd nn	−0.7	−0.7	−0.6
J_4	6.3	Kagome 3rd nn	−0.3	−0.3	−0.3
J_d	6.3	Kagome 3rd nn	24.0	19.8	16.3

TABLE IV. Exchange coupling constants for kapellasite determined from total energies of eight different spin configurations in a $2 \times 1 \times 2$ supercell. Note that here, kagome third-nearest neighbors are symmetry equivalent so that $J_4' = \frac{2}{3}J_4 + \frac{1}{3}J_d$.

Name	d_{Cu-Cu}	Type	J_i (K) $U = 6$ eV	J_i (K) $U = 7$ eV	J_i (K) $U = 8$ eV
		Kagome layer couplings			
J_1	3.15	Kagome nn	−11.8	−11.3	−10.9
J_2	5.45596	Kagome 2nd nn	−1.2	−1.0	−0.9
J_4'	6.3	Kagome 3rd nn	10.8	8.8	7.3
		Interlayer couplings			
J_3	5.733	Interlayer 1st nn	−0.4	−0.3	−0.2
J_5	6.54139	Interlayer 2nd nn	0.04	0.04	0.04
J_6	7.91421	Interlayer 3rd nn	0.04	0.04	0.03
J_8	8.51806	Interlayer 4th nn	0.01	<0.01	<0.01

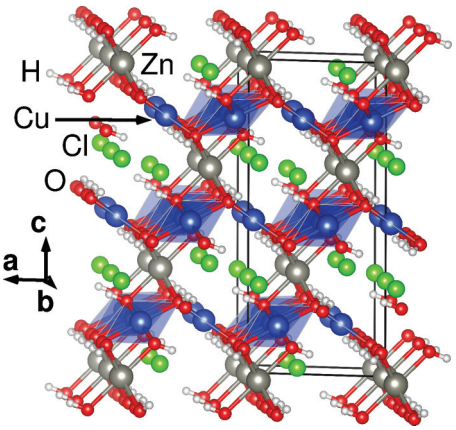

FIG. 5. (Color online) Side view of the crystal structure of herbertsmithite (approximately along the b direction).

This work was supported in part by the National Science Foundation under Grant No. NSF PHY11-25915, by the DFG through TRR/SFB 49, by the Beilstein Institut through NanoBiC, and by the Helmholtz Association through HA216/EMMI. We would like to thank A. Honecker, C. Lhuillier, P. Mendels and R. Moessner for useful discussions. Structure figures were prepared with VESTA 3.[35]

APPENDIX A: DETAILS FOR EXCHANGE CONSTANTS OF KAPELLASITE

In Tables III and IV, we provide the results of total energy calculations with GGA + U functional using different values of U. The $2 \times 1 \times 2$ supercell used in the calculation for Table IV allows resolution of four interlayer couplings of kapellasite. They are all very small, which is not surprising considering the van der Waals gap between the layers of kapellasite (see Fig. 4). This is a significant difference from the polymorph herbertsmithite that has kagome layers coupled in the third dimension via O-Zn-O bonds (see Fig. 5).

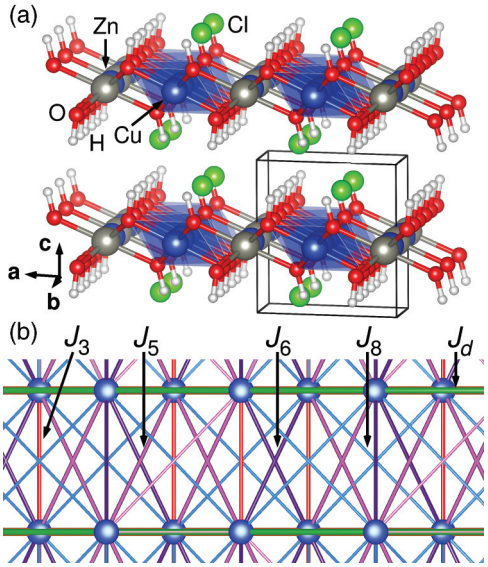

FIG. 4. (Color online) (a) Side view of the crystal structure of kapellasite (approximately along b direction). (b) Interlayer exchange paths for the Cu sites in (a).

APPENDIX B: DETAILS FOR EXCHANGE CONSTANTS OF HERBERTSMITHITE

In Table V we provide the results of total energy calculations with GGA + U functional using different values of U for $ZnCu_3(OH)_6Cl_2$.

TABLE V. Exchange coupling constants for $ZnCu_3(OH)_6Cl_2$ (herbertsmithite) determined from total energies of nine different spin configurations. Energies were calculated with GGA + U functionals at $J = 1$ eV with different values of U and with atomic-limit double-counting correction.

Name	d_{Cu-Cu}	Type	J_i (K) $U = 6$ eV	J_i (K) $U = 7$ eV	J_i (K) $U = 8$ eV
		Kagome layer couplings			
J_1	3.4171	Kagome nn	182.4	155.4	131.8
J_3	5.91859	Kagome 2nd nn	3.4	2.9	2.3
J_5	6.8342	Kagome 3rd nn	−0.4	−0.5	−0.4
		Interlayer couplings			
J_2	5.07638	Interlayer 1st nn	5.3	4.5	3.7
J_4	6.11933	Interlayer 2nd nn	−1.5	−1.1	−0.8
J_6	7.00876	Interlayer 3rd nn	−6.4	−5.4	−4.4
J_7	8.51328	Interlayer 4th nn	3.0	2.5	2.1
J_9	9.17347	Interlayer 6th nn	2.5	2.1	1.7

*jeschke@itp.uni-frankfurt.de

[1] L. Balents, Nature (London) **464**, 199 (2010).

[2] M. P. Shores, E. A. Nytko, B. M. Bartlett, and D. G. Nocera, J. Am. Chem. Soc. **127**, 13462 (2005).

[3] P. A. Lee, Science **321**, 1306 (2008).

[4] P. Mendels and F. Bert, J. Phys. Soc. Jpn. **79**, 011001 (2010).

[5] P. Mendels and F. Bert, J. Phys.: Conf. Series **320**, 012004 (2011).

[6] J. S. Helton, K. Matan, M. P. Shores, E. A. Nytko, B. M. Bartlett, Y. Yoshida, Y. Takano, A. Suslov, Y. Qiu, J.-H. Chung, D. G. Nocera, and Y. S. Lee, Phys. Rev. Lett. **98**, 107204 (2007).

[7] P. Mendels, F. Bert, M. A. de Vries, A. Olariu, A. Harrison, F. Duc, J. C. Trombe, J. S. Lord, A. Amato, and C. Baines, Phys. Rev. Lett. **98**, 077204 (2007).

[8] M. A. de Vries, J. R. Stewart, P. P. Deen, J. O. Piatek, G. J. Nilsen, H. M. Ronnow, and A. Harrison, Phys. Rev. Lett. **103**, 237201 (2009).

[9] T.-H. Han, J. S. Helton, S. Chu, D. G. Nocera, J. A. Rodriguez-Rivera, C. Broholm, and Y. S. Lee, Nature (London) **492**, 406 (2012).

[10] A. Olariu, P. Mendels, F. Bert, F. Duc, J. C. Trombe, M. A. de Vries, and A. Harrison, Phys. Rev. Lett. **100**, 087202 (2008).

[11] D. E. Freedman, T. H. Han, A. Prodi, P. Müller, Q.-Z. Huang, Y.-S. Chen, S. M. Webb, Y. S. Lee, T. M. McQueen, and D. G. Nocera, J. Am. Chem. Soc. **132**, 16185 (2010).

[12] T. Han, S. Chu, and Y. S. Lee, Phys. Rev. Lett. **108**, 157202 (2012).

[13] M. Rigol and R. R. P. Singh, Phys. Rev. Lett. **98**, 207204 (2007).

[14] L. Messio, O. Cépas, and C. Lhuillier, Phys. Rev. B **81**, 064428 (2010).

[15] A. Zorko, S. Nellutla, J. van Tol, L. C. Brunel, F. Bert, F. Duc, J.-C. Trombe, M. A. de Vries, A. Harrison, and P. Mendels, Phys. Rev. Lett. **101**, 026405 (2008).

[16] S. El Shawish, O. Cepas, and S. Miyashita, Phys. Rev. B **81**, 224421 (2010).

[17] K. Koepernik and H. Eschrig, Phys. Rev. B **59**, 1743 (1999); http://www.FPLO.de.

[18] J. P. Perdew, K. Burke, and M. Ernzerhof, Phys. Rev. Lett. **77**, 3865 (1996).

[19] H. O. Jeschke, I. Opahle, H. Kandpal, R. Valentí, H. Das, T. Saha-Dasgupta, O. Janson, H. Rosner, A. Brühl, B. Wolf, M. Lang, J. Richter, S. Hu, X. Wang, R. Peters, T. Pruschke, and A. Honecker, Phys. Rev. Lett. **106**, 217201 (2011).

[20] O. Janson, J. Richter, and H. Rosner, Phys. Rev. Lett. **101**, 106403 (2008).

[21] B. Fåk, E. Kermarrec, L. Messio, B. Bernu, C. Lhuillier, F. Bert, P. Mendels, B. Koteswararao, F. Bouquet, J. Ollivier, A. D. Hillier, A. Amato, R. H. Colman, and A. S. Wills, Phys. Rev. Lett. **109**, 037208 (2012).

[22] W. Krause, H.-J. Bernhardt, R. S. W. Braithwaite, U. Kolitsch, and R. Pritchard, Mineralog. Mag. **70**, 329 (2006).

[23] For relaxation, we use the GGA functional, $10 \times 10 \times 10$ k mesh, and optimize only the H position. We obtain the Wyckoff position (−0.199 363 675 5, 0.199 363 675 5, −0.177 444 587 6). The H-O distance is $d = 0.993$ Å.

[24] K. Foyevtsova, I. Opahle, Y. Z. Zhang, H. O. Jeschke, and R. Valenti, Phys. Rev. B **83**, 125126 (2011).

[25] B. Bernu, C. Lhuillier, E. Kermarrec, F. Bert, P. Mendels, R. H. Colman, and A. S. Wills, Phys. Rev. B **87**, 155107 (2013).

[26] T. Tay and O. I. Motrunich, Phys. Rev. B **84**, 020404(R) (2011).

[27] Y. Iqbal, F. Becca, and D. Poilblanc, New J. Phys. **14**, 115031 (2012).

[28] L. Messio, B. Bernu, and C. Lhuillier, Phys. Rev. Lett. **108**, 207204 (2012).

[29] R. Suttner, C. Platt, J. Reuther, and R. Thomale, arXiv:1303.0579.

[30] D. Schmalfuß, J. Richter, and D. Ihle, Phys. Rev. B **70**, 184412 (2004).

[31] H.-J. Schmidt, A. Lohmann, and J. Richter, Phys. Rev. B **84**, 104443 (2011); high-temperature series expansion code from http://www.uni-magdeburg.de/jschulen/HTE/.

[32] G. Misguich and P. Sindzingre, Eur. Phys. J. B **59**, 305 (2007).

[33] R. R. P. Singh and M. Rigol, J. Phys.: Conf. Series **145**, 012003 (2009).

[34] Y. Z. Zhang, H. O. Jeschke, and R. Valenti, Phys. Rev. B **78**, 205104 (2008).

[35] K. Momma and F. Izumi, J. Appl. Crystallogr. **44**, 1272 (2011).